

Multi-Marginal Gromov–Wasserstein Transport and Barycenters*

Florian Beier[†], Robert Beinert[†], and Gabriele Steidl[†]

Abstract. Gromov–Wasserstein (GW) distances are generalizations of Gromov–Hausdorff and Wasserstein distances. Due to their invariance under certain distance-preserving transformations they are well suited for many practical applications. In this paper, we introduce a concept of multi-marginal GW transport as well as its regularized and unbalanced versions. Then we generalize a bi-convex relaxation of the GW transport to our multi-marginal setting which is tight if the cost function is conditionally negative definite in a certain sense. The minimization of this relaxed model can be done by an alternating algorithm, where each step can be performed by a Sinkhorn scheme for a multi-marginal transport problem. We show a relation of our multi-marginal GW problem for a tree-structured cost function to an (unbalanced) GW barycenter problem and present different proof-of-concept numerical results.

Key words. Multi-marginal Gromov–Wasserstein transport, Gromov–Wasserstein barycenters, tight bi-convex relaxation, marginal conditionally negative definiteness.

MSC codes. 65K10, 49M20, 28A35, 28A33.

1. Introduction. Due to various applications, optimal transport (OT) and its regularized and unbalanced variants have attracted increasing attention both from the theoretical and computational point of view in recent years [27, 30]. For certain practical tasks as matching for teams [11], particle tracking [12] and information fusion [14, 15], it is useful to compute transport plans between more than two marginal measures. This is possible in the framework of multi-marginal OT [17, 26]. This problem was tackled numerically for the Coulomb cost in [6] and for repulsive costs in [13, 18]. Regularized and unbalanced variants of multi-marginal OT, which can be efficiently solved for tree-structured costs using Sinkhorn iterations, were treated in [5, 7, 19, 23]. Further, the multi-marginal OT with special cost function is closely related to the OT barycenter problem, see [1, 3, 37]. However, for some applications such as shape matching, a drawback of OT lies in the fact that it is not invariant to important invariance transformations such as translation or rotation.

A remedy are Gromov–Wasserstein (GW) distances, which were first considered by Mémoli in [25] as a modification of Gromov–Hausdorff distances and Wasserstein distances. For a survey to the geometry of Gromov–Wasserstein distances, we refer to [33]. Unbalanced GW distances were proposed in [32], a sliced version of the GW distance in [34] and a linear one in [4]. Recently, Gromov–Wasserstein distances were examined for Gaussian measures in [20, 29]. Finally, a bi-convex generalization of GW distances was introduced in [35].

The aim of this paper is i) to establish the notation of multi-marginal GW transport together with its regularized and unbalanced versions, ii) to modify the bi-convex GW distance towards the multi-marginal setting, and iii) to highlight the relation between GW barycenters

*This work was funded by the German Research Foundation (DFG) within the RTG 2433 DAEDALUS and by the BMBF project “VI-Screen” (13N15754).

[†]Institute of Mathematics, Technische Universität Berlin, Straße des 17. Juni 136, 10623 Berlin, Germany (beier@math.tu-berlin.de, beinert@math.tu-berlin.de, steidl@math.tu-berlin.de).

and multi-marginal GW transport. Its outline is as follows: in [Section 2](#), we recall basic facts on GW distances. Then, in [Section 3](#), we introduce the concept of multi-marginal GW transport. A tight relaxation of the multi-marginal GW transport is considered in [Section 4](#). In particular, we will make use of conditionally negative semi-definite kernels on tensor spaces, which we call marginal conditionally negative semi-definite. The relation of multi-marginal GW transport to the GW barycenter problem is examined in [Section 5](#) and numerical results are provided in [Section 6](#).

2. Gromov–Wasserstein Distance. A *metric measure space* (mm-space) is a triple $\mathbb{X} = (X, d, \mu)$ consisting of a compact metric space (X, d) and a Borel probability measure μ on the Borel σ -algebra induced by the metric d on X . In the following, we denote by $\mathcal{M}(X)$ the Banach space of signed Borel measures equipped with the total variation norm $\|\cdot\|_{\text{TV}}$, by $\mathcal{M}^+(X)$ the subset of positive Borel measures and by $\mathcal{P}(X)$ the subset of probability measures. Recall that a sequence $(\mu_n)_{n \in \mathbb{N}} \subset \mathcal{M}(X)$ *converges weakly* to $\mu \in \mathcal{M}(X)$, written $\mu_n \rightharpoonup \mu$, if $\int_X \varphi \, d\mu_n(x) \rightarrow \int_X \varphi \, d\mu(x)$ for all continuous functions φ on X .

For the mm-spaces $\mathbb{X}_1 = (X_1, d_1, \mu_1)$ and $\mathbb{X}_2 = (X_2, d_2, \mu_2)$, the *Gromov–Wasserstein distance* is defined by

$$(2.1) \quad \text{GW}(\mathbb{X}_1, \mathbb{X}_2) := \inf_{\pi \in \Pi(\mu_1, \mu_2)} \left(\int_{(X_1 \times X_2)^2} |d_1(x_1, x'_1) - d_2(x_2, x'_2)|^2 \, d\pi(x_1, x_2) \, d\pi(x'_1, x'_2) \right)^{\frac{1}{2}},$$

where $\Pi(\mu_1, \mu_2) \subset \mathcal{P}(X_1 \times X_2)$ consists of all measures with marginals μ_1 and μ_2 . By [[25](#), Cor 10.1], the infimum in (2.1) is attained by some optimal GW transport plan π^* , which is in general not unique. Further, $\text{GW}(\mathbb{X}_1, \mathbb{X}_2) = 0$ if and only if there exists a measure-preserving isometry $\mathcal{I}: X_1 \rightarrow X_2$ with $\mu_2 = \mathcal{I}_\# \mu_1 := \mu_1 \circ \mathcal{I}^{-1}$. The GW distance defines a metric on the quotient space of mm-spaces with respect to measure-preserving isometries [[25](#), Thm 5.1].

Instead of fixing the marginals of the transport plan, S ejourn e, Vialard, and Peyr e [[32](#)] transferred the concept of unbalanced OT [[22](#)] to the GW setting by penalizing the divergences between the marginals and the given measures. To this end, recall that, for a so-called *entropy function*, i.e. a convex and lower semi-continuous functions $\phi: \mathbb{R}_{\geq 0} \rightarrow [0, \infty]$ satisfying $\phi(1) = 0$, and two measures $\mu, \nu \in \mathcal{M}^+(X)$ with Radon–Nikod ym decomposition $\mu = d\mu/d\nu + \mu^\perp$, the (*Csisz ar*) ϕ -divergence is given by

$$D_\phi(\mu, \nu) = \int_X \phi\left(\frac{d\mu}{d\nu}\right) d\nu + \phi'_\infty \int_X d\mu^\perp$$

with the convention $0 \cdot \infty = 0$ and the *recession constant* $\phi'_\infty := \lim_{x \rightarrow \infty} \phi(x)/x$. Let $\phi: \mathbb{R}_{\geq 0} \rightarrow [0, \infty]$ be an entropy function. Then D_ϕ is jointly convex, weakly lower semi-continuous, and non-negative, see [[22](#), Cor 2.9]. In this paper, we will apply the ϕ -divergences given in [Table 1](#). In particular, for the Boltzman–Shannon entropy $\phi(t) := t \log(t) - t + 1$, we obtain the *Kullback–Leibler (KL) divergence*

$$\text{KL}(\mu, \nu) := \begin{cases} \int \log\left(\frac{d\mu}{d\nu}\right) d\nu - \mu(X) + \nu(X), & \mu \ll \nu, \\ \infty, & \text{else.} \end{cases}$$

Table 1

Entropy functions ϕ with recession constant ϕ'_∞ and corresponding ϕ -divergences.

	$\phi(t)$	ϕ'_∞	$D_\phi(\mu, \nu)$
balanced (ϕ_{bal})	$\iota_{\{1\}}(t)$	∞	$\iota_{\{\nu\}}(\mu)$
unconstrained (ϕ_{free})	$\iota_{[0, \infty)}(t)$	0	0
Kullback–Leibler (ϕ_{ent})	$t \log(t) - t + 1$	∞	$\text{KL}(\mu, \nu)$

The *regularized, unbalanced GW transport* [32] is given for $\varepsilon \geq 0$ by

$$\text{UGW}_\varepsilon(\mathbb{X}_1, \mathbb{X}_2) := \inf_{\pi \in \mathcal{M}^+(X_1 \times X_2)} \left(\int_{X^2} |d_1 - d_2|^2 d\pi + \sum_{i=1}^2 D_{\phi_i}^\otimes(\pi_i, \mu_i) + \varepsilon \text{KL}^\otimes(\pi, \mu_1 \otimes \mu_2) \right)^{\frac{1}{2}}$$

with $D_{\phi_i}^\otimes(\mu, \nu) := D_{\phi_i}(\mu \otimes \mu, \nu \otimes \nu)$ and marginals $\pi_i := (P_i)_\# \pi$, where $P_i(x_1, x_2) := x_i$, $i = 1, 2$. We use similar notations for projections onto the components of higher-order Cartesian products. Depending on the chosen divergence, the marginals of the computed plan may match the given μ_i (balanced), be close to them (scaled Kullback–Leibler), or completely free (unconstrained). To keep the notation simple, we used $\mu_1 \otimes \mu_2$ in the KL divergence. However, this could be replaced by the the product of Lebesgue measures or counting measures on the respective spaces, see [5].

3. Multi-marginal Gromov–Wasserstein Transport. Towards a multi-marginal GW setting, we consider a series of mm-spaces $\mathbb{X}_i = (X_i, d_i, \mu_i)$, $i = 1, \dots, N$. The Cartesian product of the domains is henceforth denoted by $X := \times_{i=1}^N X_i$. We then introduce the *multi-marginal GW transport* problem as

$$\text{MGW}(\mathbb{X}_1, \dots, \mathbb{X}_N) := \inf_{\pi \in \Pi(\mu_1, \dots, \mu_N)} \int_{X^2} c(x, x') d\pi(x) d\pi(x'),$$

where $\pi \in \Pi(\mu_1, \dots, \mu_N) := \{\pi \in \mathcal{P}(X) : (P_i)_\# \pi = \mu_i\}$ and $c: X \times X \rightarrow [0, \infty]$. A typical cost function is

$$(3.1) \quad c(x, x') := \sum_{i,j=1}^N c_{ij} |d_i(x_i, x'_i) - d_j(x_j, x'_j)|^2 \quad \text{with} \quad c_{ij} \geq 0.$$

In analogy to the unbalanced GW transport, we consider for $\varepsilon \geq 0$, the *regularized, unbalanced multi-marginal GW transport* problem

$$\text{UMGW}_\varepsilon(\mathbb{X}_1, \dots, \mathbb{X}_N) := \inf_{\pi \in \mathcal{M}^+(X)} \underbrace{\int_{X^2} c(x, x') d\pi(x) d\pi(x') + \sum_{i=1}^N D_{\phi_i}^\otimes(\pi_i, \mu_i) + \varepsilon \text{KL}^\otimes(\pi, \mu^\otimes)}_{=: F_\varepsilon(\pi)},$$

where $\mu^\otimes := \mu_1 \otimes \dots \otimes \mu_N$. Under mild conditions, the infimum is attained.

Proposition 3.1 (Existence of Minimizer). *Let the cost function $c: X \times X \rightarrow \mathbb{R}_+$ be lower semi-continuous. Assume either $\varepsilon > 0$ or $\sum_{i=1}^N (\phi_i)'_\infty > 0$. Then UMGW_ε is finite and the infimum is attained.*

The statement can be shown by following the lines in the proof of [32, Prop. 7]. To make the paper self-contained, we give the proof in the appendix.

4. Bi-convex Relaxation. In this section, we consider a bi-convex relaxation of UMGW_ε . If the cost function belongs to a certain class of conditionally negative definite functions, then we will see that the relaxation of the balanced problem becomes tight. We introduce this class of cost functions, before we deal with the bi-convex relaxation.

4.1. Conditionally Negative Semi-definiteness. In the following, we consider the results from [35] and [24] from a multi-marginal point of view. Recall that a symmetric matrix $A \in \mathbb{R}^{d \times d}$ is *negative semi-definite* if $\alpha^\top A \alpha \leq 0$ for all $\alpha = (\alpha(i))_{i=1}^d \in \mathbb{R}^d$. This is equivalent to the fact that A has only non-positive eigenvalues. Further, $A \in \mathbb{R}^{d \times d}$ is *negative semi-definite* on a subspace $V \subset \mathbb{R}^d$ if $v^\top A v \leq 0$ for all $v \in V$. If the columns of $B \in \mathbb{R}^{d \times \dim V}$ form an orthonormal basis of V , this is equivalent to $\alpha^\top B^\top A B \alpha \leq 0$ for all $\alpha \in \mathbb{R}^{\dim V}$, i.e. to the negative semi-definiteness of $B^\top A B \in \mathbb{R}^{\dim V \times \dim V}$.

A continuous, symmetric function $k: X \times X \rightarrow \mathbb{R}$ is *negative definite*, if for all points $x^1, \dots, x^d \in X$ and all $d \in \mathbb{N}$, the matrix $(k(x^m, x^n))_{m,n=1}^d$, is negative semi-definite and *conditionally negative definite* (of order 1) if this holds true on the subspace

$$V_{\mathbf{1}_d} := \{\alpha := (\alpha(j))_{j=1}^d \in \mathbb{R}^d : \alpha^\top \mathbf{1}_d = 0\},$$

see [31, 38]. Typical conditionally negative definite functions are $\|x - y\|_2$ on compact subsets of \mathbb{R}^d and spherical distances $d(x, y)$ [9]. For further examples, we refer to [16]. We will need the following auxiliary lemma.

Lemma 4.1. *Let $A_i \in \mathbb{R}^{d_i \times d_i}$, and let $V_i \subset \mathbb{R}^{d_i}$ be subspaces for $i = 1, 2$. Then $-(A_1 \otimes A_2)$ is conditionally negative semi-definite on $V_1 \otimes V_2$ if and only if either A_i , $i = 1, 2$, or $-A_i$, $i = 1, 2$, are conditionally negative semi-definite on V_i , $i = 1, 2$.*

Proof. Let $B_i \in \mathbb{R}^{d_i \times \dim V_i}$ be matrices whose columns form an orthonormal bases of V_i , $i = 1, 2$. Then $B_1 \otimes B_2$ is a basis of $V_1 \otimes V_2$ and $-(A_1 \otimes A_2)$ is conditionally negative semi-definite on $V_1 \otimes V_2$ if and only if

$$-(B_1 \otimes B_2)^\top (A_1 \otimes A_2) (B_1 \otimes B_2) = -(B_1^\top A_1 B_1) \otimes (B_2^\top A_2 B_2)$$

is negative semi-definite. Considering that the eigenvalues on the right-hand side are the negative pairwise products of the eigenvalues of $B_i^\top A_i B_i$, $i = 1, 2$, we obtain the assertion. ■

In our application, the cost function is given on the compact Cartesian space $X := \times_{i=1}^N X_i$, $N \geq 2$ and often has a special structure as those in (3.1). This gives rise to the following definition. For $M = (M_i)_{i=1}^N \in \mathbb{N}^N$, let $[M] := \{m = (m_1, \dots, m_N) \in \mathbb{N}^N : 1 \leq m_i \leq M_i\}$. A continuous, symmetric function $c: X \times X \rightarrow \mathbb{R}$ is called *marginal conditionally negative definite* if

$$(4.1) \quad \sum_{m,n \in [M]} c(x^m, x^n) \alpha(x^m) \alpha(x^n) \leq 0, \quad x^m := (x_1^{m_1}, \dots, x_N^{m_N}) \in \times_{i=1}^N \mathcal{X}_i,$$

for all $\mathcal{X}_i := \{x_i^{m_i} \in X_i : m_i = 1, \dots, M_i\}$, $M \in \mathbb{N}^N$ and for all $\alpha \in \mathcal{M}(\times_{i=1}^N \mathcal{X}_i)$ satisfying $(P_i)_\# \alpha \equiv 0$ for $1 \leq i \leq N$. Clearly, a conditionally negative definite function is marginal conditionally negative definite, but not conversely. Then we have the following proposition.

Proposition 4.2. *Let $c: X \times X \rightarrow \mathbb{R}$ be defined by (3.1), where d_i , $i = 1, \dots, N$ are conditionally negative semi-definite functions. Then c is marginal conditionally negative definite.*

Proof. Since the sum of marginal conditionally negative definite functions keeps this property, it remains to restrict our attention to the function

$$|d_i(x_i, x'_i) - d_j(x_j, x'_j)|^2 = d_i^2(x_i, x'_i) + d_j^2(x_j, x'_j) - 2d_i(x_i, x'_i)d_j(x_j, x'_j).$$

By definition of α , we have that

$$\sum_{m, n \in [M]} d_i^2(x_i^{m_i}, x_i^{n_i}) \alpha(x^m) \alpha(x^n) = \sum_{m_i, n_i} d_i^2(x_i^{m_i}, x_i^{n_i}) [(P_i)_\# \alpha](x_i^{m_i}) [(P_i)_\# \alpha](x_i^{n_i}) = 0$$

and that $-d_i(x_i, x'_i)d_j(x_j, x'_j)$ is negative semi-definite on $X \times X$ if and only if this is true on $(X_i \times X_j) \times (X_i \times X_j)$. For the latter, it remains to show that $-(d_i(x_i^{m_i}, x_i^{n_i}))_{m_i, n_i=1}^{M_i} \otimes (d_j(x_j^{m_j}, x_j^{n_j}))_{m_j, n_j=1}^{M_j}$ is negative semi-definite on $V_{\mathbf{1}_{M_i}} \otimes V_{\mathbf{1}_{M_j}}$. By Lemma 4.1 this is indeed the case. \blacksquare

4.2. Tight Bi-convex Relaxation. The objective F_ε in UMGW_ε is quadratic in π . Inspired from [32] for GW distances, we propose the following bi-convex relaxation to tackle UMGW_ε numerically:

$$\begin{aligned} & \text{UMGW}_\varepsilon^{\text{bi}}(\mathbb{X}_1, \dots, \mathbb{X}_N) \\ & := \inf_{\pi, \gamma \in \mathcal{M}^+(X)} \underbrace{\int_{X^2} c(x, x') d\pi(x) d\gamma(x') + \sum_{i=1}^N D_{\phi_i}(\pi_i \otimes \gamma_i, \mu_i \otimes \mu_i) + \varepsilon \text{KL}(\pi \otimes \gamma, (\mu^\otimes)^2)}_{=: F_\varepsilon^{\text{bi}}(\pi, \gamma)}. \end{aligned}$$

By construction, the relaxation always satisfies $\text{UMGW}_\varepsilon^{\text{bi}} \leq \text{UMGW}_\varepsilon$. Moreover, in the balanced case, it becomes tight for marginal conditionally negative definite cost functions, meaning that any minimizer (π^*, γ^*) of $\text{UMGW}_\varepsilon^{\text{bi}}$ yields the minimizers π^* and γ^* of UMGW_ε .

Proposition 4.3 (Tightness of Relaxation). *Let $\phi_i := \phi_{\text{bal}}$, $i = 1, \dots, N$, $\varepsilon \geq 0$ and c be marginal conditionally negative definite. Then, $\text{UMGW}_\varepsilon = \text{UMGW}_\varepsilon^{\text{bi}}$ and every minimizer (π^*, γ^*) of $\text{UMGW}_\varepsilon^{\text{bi}}$ satisfies*

$$(4.2) \quad F_\varepsilon^{\text{bi}}(\pi^*, \gamma^*) = F_\varepsilon^{\text{bi}}(\pi^*, \pi^*) = F_\varepsilon^{\text{bi}}(\gamma^*, \gamma^*)$$

such that π^* and γ^* are minimizers of UMGW_ε .

Proof. The balanced setting ensures that all occurring measures are probability measures. The KL divergence then splits into $\text{KL}(\pi \otimes \gamma, \mu^\otimes \otimes \mu^\otimes) = \text{KL}(\pi, \mu^\otimes) + \text{KL}(\gamma, \mu^\otimes)$ by [32, Prop 9]. Further, the values in (4.2) always satisfy

$$F_\varepsilon^{\text{bi}}(\pi^*, \gamma^*) \leq F_\varepsilon^{\text{bi}}(\pi^*, \pi^*) \quad \text{and} \quad F_\varepsilon^{\text{bi}}(\pi^*, \gamma^*) \leq F_\varepsilon^{\text{bi}}(\gamma^*, \gamma^*)$$

Incorporating the KL splitting, and defining $K(\pi, \gamma) := \int_{X^2} c \, d\pi \, d\gamma$ and $f(\pi) := \text{KL}(\pi, \mu^\otimes)$, we obtain

$$\begin{aligned} K(\pi^*, \gamma^*) + \varepsilon f(\pi^*) + \varepsilon f(\gamma^*) &\leq K(\pi^*, \pi^*) + 2\varepsilon f(\pi^*), \\ K(\pi^*, \gamma^*) + \varepsilon f(\pi^*) + \varepsilon f(\gamma^*) &\leq K(\gamma^*, \gamma^*) + 2\varepsilon f(\gamma^*). \end{aligned}$$

Now, assume that (4.2) is false, i.e. at least one of these inequalities is strict. Adding both inequalities then yields

$$(4.3) \quad 0 < K(\pi^* - \gamma^*, \pi^* - \gamma^*) = K(\alpha, \alpha) \quad \text{with} \quad \alpha := \pi^* - \gamma^*.$$

Since $\pi^*, \gamma^* \in \Pi(\mu_1, \dots, \mu_N)$, we have $(P_i)_\# \alpha \equiv 0$, $i = 1, \dots, N$. Then the marginally conditionally negative definiteness of c ensures $K(\alpha, \alpha) \leq 0$. This is however a contradiction to (4.3). \blacksquare

Note that the proposition does not immediately follow from [32, Thm 2] since the proof given there is not reproducible for us in the non-definite case. More precisely, $x^\top A x = 0$, $x^\top \mathbf{1} = \mathbf{0}$ does not imply for a conditionally negative semi-definite matrix A that $x \in \ker A$.

The bi-convex relaxation UMGW_ε encourages to use an alternating minimization scheme over π and γ . The minimization over one variable here corresponds to multi-marginal optimal transport problems with very specific cost functions. In the following proposition, we restrict our attention to the KL divergence. The other divergences from Table 1 may be exploited analogously.

Proposition 4.4. *Let $\phi_i = \phi_{\text{ent}}$, $i = 1, \dots, N$. Then, for fixed $\gamma \in \mathcal{M}^+(X)$, the minimization over π in $\text{UMGW}_\varepsilon^{\text{bi}}$ becomes the multi-marginal transport problem*

$$\operatorname{argmin}_{\pi \in \mathcal{M}^+(X)} F_\varepsilon^{\text{bi}}(\pi, \gamma) := \int_X c_\gamma(x) \, d\pi(x) + \|\gamma\|_{\text{TV}} \sum_{i=1}^N \text{KL}(\pi_i, \mu_i) + \varepsilon \|\gamma\|_{\text{TV}} \text{KL}(\pi, \mu^\otimes),$$

with

$$c_\gamma(x) := \int_X c(x, x') \, d\gamma(x') + \sum_{i=1}^N \int_{X_i} \log\left(\frac{d\gamma_i}{d\mu_i}\right) \, d\gamma_i + \varepsilon \int_X \log\left(\frac{d\gamma}{d\mu^\otimes}\right) \, d\gamma.$$

Proof. Using the factorization of the KL divergence in [32, Prop 9] and the definition of Csiszár's divergences, we obtain for arbitrary measures $\alpha_1, \alpha_2, \alpha_3 \in \mathcal{M}^+(Y)$ that

$$\text{KL}(\alpha_1 \otimes \alpha_2, \alpha_3 \otimes \alpha_3) = \int_Y \int_Y \log\left(\frac{d\alpha_2}{d\alpha_3}\right) \, d\alpha_2 \, d\alpha_1 + \|\alpha_2\|_{\text{TV}} \text{KL}(\alpha_1, \alpha_3) - \|\alpha_2\|_{\text{TV}} \|\alpha_3\|_{\text{TV}} + \|\alpha_3\|_{\text{TV}}^2.$$

Applying this to all KL terms in $F_\varepsilon^{\text{bi}}$, we obtain

$$\begin{aligned} F_\varepsilon^{\text{bi}}(\pi, \gamma) &= \int_{X^2} c(x, x') \, d\pi(x) \, d\gamma(x') \\ &\quad + \sum_{i=1}^N \left(\int_X \int_{X_i} \log\left(\frac{d\gamma_i}{d\mu_i}\right) \, d\gamma_i \, d\pi + \underbrace{\|\mu_i\|_{\text{TV}}^2 - \|\gamma_i\|_{\text{TV}} \|\mu_i\|_{\text{TV}}}_{\text{constant}} \right) \end{aligned}$$

$$+ \varepsilon \left(\int_X \int_X \log\left(\frac{d\gamma}{d\mu^\otimes}\right) d\gamma d\pi + \|\gamma\|_{\text{TV}} \text{KL}(\pi, \mu^\otimes) + \underbrace{\|\mu^\otimes\|_{\text{TV}}^2 - \|\gamma\|_{\text{TV}} \|\mu^\otimes\|_{\text{TV}}}_{\text{constant}} \right).$$

Rearranging terms and omitting the constant terms yields the assertion. \blacksquare

The minimization of $F_\varepsilon^{\text{bi}}(\cdot, \gamma)$ over $\mathcal{M}^+(X)$ may be efficiently solved using the multi-marginal Sinkhorn scheme in [5] if the cost function has a sparse structure. For example, we can use cost functions of the form (3.1) with $N - 1$ non-zero coefficients c_{ij} such that (3.1) decouples according to a tree.

5. Barycenters. Barycenters and multi-marginal optimal transports are closely related [3, 5, 11, 19]. For the GW setting, we obtain similar results. For $\rho_i \geq 0$ with $\sum_{i=1}^N \rho_i = 1$, a *Gromov–Wasserstein barycenter* between the mm-spaces $\mathbb{X}_i := (X_i, d_i, \mu_i)$, $i = 1, \dots, N$, is a minimizing mm-space $\mathbb{Y} := (Y, d, \nu)$ of

$$(5.1) \quad \inf_{\mathbb{Y}} \sum_{i=1}^N \rho_i \text{GW}^2(\mathbb{X}_i, \mathbb{Y}).$$

Theorem 5.1 (Free-Support Barycenter). *Let \mathbb{X}_i be given mm-spaces, and let $\rho_i \geq 0$ be weights with $\sum_{i=1}^N \rho_i = 1$. Then a Gromov–Wasserstein barycenter $\mathbb{Y}^* := (Y^*, d^*, \nu^*)$ is given by $Y^* = \times_{i=1}^N X_i$, $d^*(x, x') = \sum_{i=1}^N \rho_i d_i(x_i, x'_i)$, and $\nu^* = \pi^*$, where π^* is a minimizer of $\text{MGW}(\mathbb{X}_1, \dots, \mathbb{X}_N)$ with cost function*

$$c(x, x') := \frac{1}{2} \sum_{i,j=1}^N \rho_i \rho_j |d_i(x_i, x'_i) - d_j(x_j, x'_j)|^2.$$

Proof. First we note that the cost function may be rearranged as

$$c(x, x') = \sum_{i=1}^N \rho_i d_i^2(x_i, x'_i) - \sum_{i,j=1}^N \rho_i \rho_j d_i(x_i, x'_i) d_j(x_j, x'_j) = \sum_{i=1}^N \rho_i \left| d_i(x_i, x'_i) - \overbrace{\sum_{j=1}^N \rho_j d_j(x_j, x'_j)}^{=d^*(x, x')} \right|^2$$

Let \mathbb{Y} be an arbitrary minimizer of (5.1), and let $\pi_{\text{GW}}^{(i)}$ be an optimal plan of $\text{GW}(\mathbb{X}_i, \mathbb{Y})$. Since all these plans have the marginal $(P_2)_\# \pi_{\text{GW}}^{(i)} = \nu$, Dudley’s lemma [2, Lem 8.4] ensures the existence of a gluing $\pi_g \in \Pi(\mu_1, \dots, \mu_N, \nu)$ with $(P_{X_i \times Y})_\# \pi_g = \pi_{\text{GW}}^{(i)}$. Exploiting that the 2-marginals of π_g are optimal Gromov–Wasserstein plans, and that the mean $d^*(x, x')$ is the pointwise minimizer of $\min_{t \in \mathbb{R}} \sum_{i=1}^N \rho_i |d_i(x_i, x'_i) - t|^2$ for fixed x and x' , we obtain

$$(5.2) \quad \begin{aligned} \sum_{i=1}^N \rho_i \text{GW}^2(\mathbb{X}_i, \mathbb{Y}) &= \int_{(X \times Y)^2} \sum_{i=1}^N \rho_i |d_i(x_i, x'_i) - d(y, y')|^2 d\pi_g(x, y) d\pi_g(x', y') \\ &\geq \int_{(X \times Y)^2} \underbrace{\sum_{i=1}^N \rho_i |d_i(x_i, x'_i) - d^*(x, x')|^2}_{=c(x, x')} d\pi_g(x, y) d\pi_g(x', y') \geq \text{MGW}(\mathbb{X}_1, \dots, \mathbb{X}_N), \end{aligned}$$

where we exploit $(P_X)_{\#}\pi_g \in \Pi(\mu_1, \dots, \mu_N)$ in the last step. Using the substitutions $\pi_*^{(i)} := (P_{X_i}, \text{id})_{\#}\pi^*$ for any optimal plan π^* of MGW, we further have

$$\begin{aligned} \text{MGW}(\mathbb{X}_1, \dots, \mathbb{X}_N) &= \sum_{i=1}^N \rho_i \int_{X^2} |d_i(x_i, x'_i) - d^*(x, x')|^2 d\pi^*(x) d\pi^*(x') \\ &= \sum_{i=1}^N \rho_i \int_{X_i \times X} |d_i(x_i, x'_i) - d^*(y, y')|^2 d\pi_*^{(i)}(x_i, y) d\pi_*^{(i)}(x'_i, y') \geq \sum_{i=1}^N \rho_i \text{GW}^2(\mathbb{X}_i, \mathbb{Y}^*). \end{aligned}$$

Due to (5.2), the last inequality has to be an equality showing that $\mathbb{Y}^* = (Y^*, d^*, \nu^*)$ from the assertion is in fact a barycenter between $\mathbb{X}_1, \dots, \mathbb{X}_N$. \blacksquare

In the special case $N = 2$, the barycenters from Theorem 5.1 have the form $(X_1 \times X_2, (1 - \rho)d_1 + \rho d_2, \pi^*)$, where π^* is an optimal plan of GW. For a fixed π^* , we thus obtain a geodesic in the GW space [33, Thm 3.1]. Although Theorem 5.1 allows us to determine barycenters between arbitrary spaces, due to the generality of the mm-space \mathbb{Y} , these barycenters are difficult to interpret since \mathbb{Y} can have a completely different structure than \mathbb{X}_i . However, for GW barycenters with respect to images for instance, we would, expect to obtain again an image. In this situation, it therefore makes sense to fix (Y, d) in \mathbb{Y} and to minimize only over the measure ν . Moreover, the GW barycenter may be relaxed by considering unbalanced transport. Against this background, we consider the *fixed-support (unbalanced) Gromov–Wasserstein barycenter* given by

$$(5.3) \quad \operatorname{argmin}_{\nu \in \mathcal{M}^+(Y)} \sum_{i=1}^N \rho_i \text{UGW}^2(\mathbb{X}_i, \mathbb{Y}) \quad \text{with} \quad \mathbb{Y} = (Y, d, \nu),$$

where the UGW terms may be unbalanced in \mathbb{X}_i with respect to some entropy function ϕ_i and is balanced with respect to \mathbb{Y} . The procedure for computing GW barycenters proposed in [28] does exactly the opposite: the measure ν of \mathbb{Y} is fixed beforehand and the optimization is done over the metric space (Y, d) .

Theorem 5.2 (Fixed-Support Barycenter). *Let \mathbb{X}_i be given mm-spaces, and $\rho_i \geq 0$ be weights with $\sum_{i=1}^N \rho_i = 1$. A fixed-support (unbalanced) Gromov–Wasserstein barycenter $\mathbb{Y}^* := (Y, d, \nu^*)$ is given by $\nu^* = (P_Y)_{\#}\pi^*$, where π^* minimizes $\text{UMGW}(\mathbb{X}_1, \dots, \mathbb{X}_N, \mathbb{Y})$ with cost function*

$$c((x, y), (x', y')) := \sum_{i=1}^N \rho_i |d_i(x_i, x'_i) - d(y, y')|^2.$$

The unregularized UMGW is here unbalanced in \mathbb{X}_i with respect to $\rho_i \phi_i$ and unrestricted in \mathbb{Y} .

Proof. The assertion may be established similarly to Theorem 5.1. First, let \mathbb{Y} and thus ν be an arbitrary minimizer of (5.3), and let $\pi_{\text{UGW}}^{(i)}$ be an optimal plan of $\text{UGW}(\mathbb{X}_i, \mathbb{Y})$, $i = 1, \dots, N$. Since the UGW problems are balanced in \mathbb{Y} , all these plans have the marginal $(P_2)_{\#}\pi_{\text{UGW}}^{(i)} = \nu$. Again, Dudley’s lemma [2, Lem 8.4] ensures the existence of a gluing $\pi_g \in$

$\Pi(\mu_1, \dots, \mu_N, \nu)$ with $(P_{X_i \times Y})_{\#} \pi_g = \pi_{\text{UGW}}^{(i)}$. Based on this gluing, we obtain

$$\begin{aligned}
 (5.4) \quad \sum_{i=1}^N \rho_i \text{UGW}^2(\mathbb{X}_i, \mathbb{Y}) &= \sum_{i=1}^N \rho_i \left(\int_{(X \times Y)^2} |d_i - d|^2 d\pi_g d\pi_g + D_{\phi_i}^{\otimes}((P_{X_i})_{\#} \pi_g, \mu_i) \right) \\
 &= \int_{(X \times Y)^2} \underbrace{\sum_{i=1}^N \rho_i |d_i - d|^2}_{=c} d\pi_g d\pi_g + \sum_{i=1}^N \rho_i D_{\phi_i}^{\otimes}((P_{X_i})_{\#} \pi_g, \mu_i) \geq \text{UMGW}(\mathbb{X}_1, \dots, \mathbb{X}_N, \mathbb{Y}),
 \end{aligned}$$

where UMGW is unrestricted in \mathbb{Y} . Considering the marginals $\pi_*^{(i)} := (P_{X_i \times Y})_{\#} \pi^*$ of any optimal UMGW plan π^* , whose second marginals coincide, we further have

$$\begin{aligned}
 \text{UMGW}(\mathbb{X}_1, \dots, \mathbb{X}_N, \mathbb{Y}) &= \sum_{i=1}^N \rho_i \left(\int_{(X_i \times Y)^2} |d_i - d|^2 d\pi_*^{(i)} d\pi_*^{(i)} + D_{\phi_i}^{\otimes}((P_1)_{\#} \pi_*^{(i)}, \mu_i) \right) \\
 &\geq \sum_{i=1}^N \rho_i \text{UGW}^2(\mathbb{X}_i, \mathbb{Y}).
 \end{aligned}$$

The last inequality has to be an equality because of (5.4), so \mathbb{Y} with $\nu^* = (P_Y)_{\#} \pi^*$ is a fixed-support barycenter. \blacksquare

6. Numerical Examples. The multi-marginal GW transport is especially useful for image processing tasks like the computation of barycenters or progressive interpolations and for noise removal. We consider (gray-value) images on $[-1/2, 1/2]^2$, which may be described as piecewise constant functions on its pixel grid. These images can be interpreted as discrete mm-spaces $\mathbb{X} = (X, d, \mu)$, where X is the grid containing the centers of the pixels, d is the Euclidian distance, and μ is the probability measure corresponding to the (normalized) gray values.

6.1. Balanced and Unbalanced Barycenters. In the first example, we set $\rho_1 = \rho_2 = \frac{1}{2}$ and consider the outlines of circle \mathbb{X}_1 and rectangle \mathbb{X}_2 , see Figure 1. Each image and the unknown barycenter \mathbb{Y} initially consists of 64×64 pixels. To determine a barycenter (5.3), we employ the multi-marginal GW transport in Theorem 5.2 computed by the bi-convex relaxation and the multi-marginal Sinkhorn scheme [5]. The minimizer π^* of $\text{UMGW}_{\varepsilon}(\mathbb{X}_1, \mathbb{X}_2, \mathbb{Y})$ (balanced in $\mathbb{X}_1, \mathbb{X}_2$, unrestricted in \mathbb{Y}) is numerically determined using a small regularization $\varepsilon = 0.0004$ with respect to the counting measure on $X_1 \times X_2 \times Y$. Figure 1 shows the approximate barycenter $\nu^* := (P_Y)_{\#} \pi^*$ in form of a rounded rectangle. The result is slightly blurred as usual when using the Sinkhorn scheme.

To speed-up the computations, the given mm-spaces \mathbb{X}_1 and \mathbb{X}_2 are restricted to non-zero pixels. Since the main bottleneck is now the number of points in \mathbb{Y} , we use a *multilevel approach*. First, we compute a rough barycenter on mere 8×8 pixels. Then, we divide each non-zero pixel (greater than 0.001) into 4 subpixels and add the 8-neighborhood of these subpixels. Next, a barycenter on the corresponding subset of the 16×16 grid is computed. Repeating this refinement several times, we finally obtain an approximate barycenter on the desired 64×64 grid. Where the computation on the full 64×64 grid takes 31 seconds, the

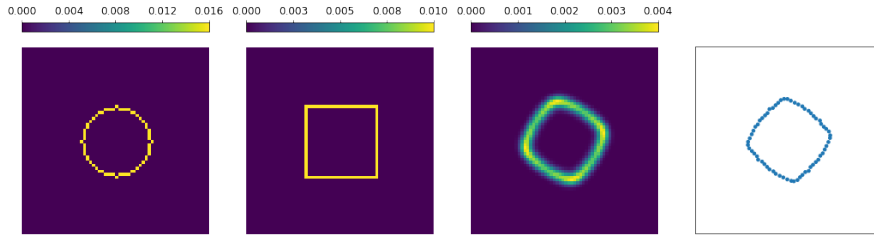


Figure 1. Left to right: The given marginals with respect to circle \mathbb{X}_1 and rectangle \mathbb{X}_2 . Computed barycenter \mathbb{Y} using [Theorem 5.2](#). Embedded barycenter using [\[28\]](#).

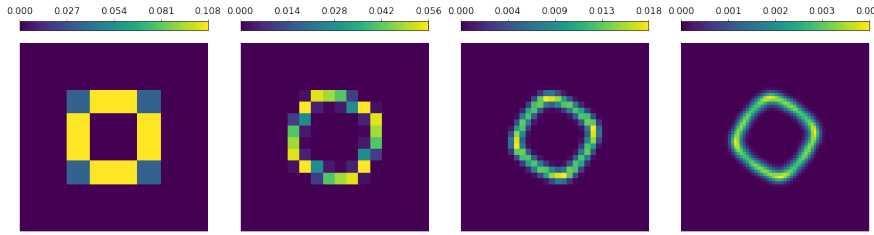


Figure 2. Four barycenters computed by a multiscale scheme.

multilevel approach require only 6 seconds at all. The intermediate barycenters are shown in [Figure 2](#).

For comparison, we apply the barycenter algorithm of Peyré, Cuturi, and Solomon [\[28\]](#). Different from our approach, the measure of \mathbb{Y} is here given beforehand, and the minimization is performed with respect to the metric space. More precisely, the algorithm determines a minimizing metric between the discrete points. The computed metric space with respect to the uniform distribution on 64 points is then embedded into \mathbb{R}^2 and shows a similar structure to our method, see [Figure 1](#).

To emphasize the differences between the balanced and unbalanced case as well as to the Wasserstein setting, we consider a further instance of this example whose inputs are shown in [Figure 3](#). Using a regularization by $\varepsilon = 0.0003$, we compute as before a balanced barycenter. Because the GW distance is invariant under isometries, it is here beneficial to map circle and rectangle as well as cross and triangle. Figuratively, the algorithm computes the pairwise barycenters between the objects that are more similar to each other. Since the outlines have different masses, there occurs a small artifact in the middle of the image. This artifact does not appear in the unbalanced GW barycenter, where the marginals are penalized using $\phi_i = 0.1 \phi_{\text{ent}}$, $i = 1, 2$. As comparison, we have also computed the balanced and unbalanced Wasserstein barycenters using the algorithm in [\[5\]](#). Here the shapes are averaged as they occur. The power of the GW approach is the independence with respect to shifts, rotations and reflections—the barycenter always looks the same—whereas the Wasserstein barycenter will significantly change.

6.2. Progressive Interpolation. For this example, we take two 2D shapes represented by (50×50) -pixel images from the publicly available database [\[10\]](#). The aim is to show that

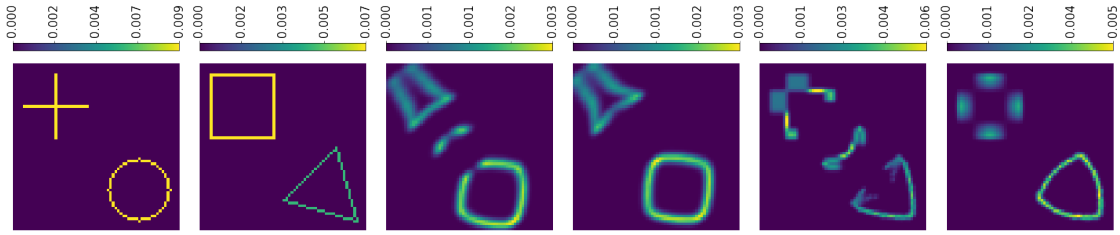


Figure 3. Left to right: The given marginals with respect to cross/circle \mathbb{X}_1 and rectangle/triangle \mathbb{X}_2 . Computed balanced and unbalanced GW barycenter \mathbb{Y} using [Theorem 5.2](#). Computed balanced and unbalanced Wasserstein barycenter using [\[5\]](#).

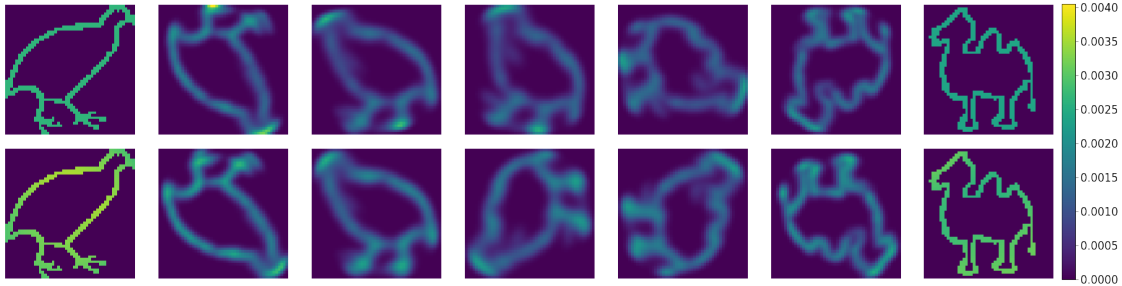


Figure 4. Progressive Gromov–Wasserstein interpolation via multi-marginal Gromov–Wasserstein transport in the balanced (top row) and unbalanced (bottom row) setting.

multi-marginal transport can be used to compute a progressive interpolation consisting of several intermediate images. Mathematically, \mathbb{X}_1 (bird) and \mathbb{X}_N (camel) are known, and the intermediate images \mathbb{X}_i , $i = 2, \dots, N - 1$, should be close to their neighbours with respect to the GW distance. For this reason, we use the cost function

$$c = \sum_{i=1}^{N-1} |d_i - d_{i+1}|^2,$$

where d_i is the Euclidean distance on \mathbb{R}^2 . Similarly to the fixed-support barycenter in [Theorem 5.2](#), we consider hard marginal constraints on \mathbb{X}_1 and \mathbb{X}_N ($\phi_1 = \phi_N = \phi_{\text{bal}}$) for the balanced and KL divergence ($\phi_1 = \phi_N = 0.02 \phi_{\text{ent}}$) for the unbalanced setting. In both cases, we set no penalization on $\mathbb{X}_2, \dots, \mathbb{X}_{N-1}$ ($\phi_2 = \dots = \phi_{N-1} = \phi_{\text{free}}$). The free marginals of the minimizing UMGW plans are shown in [Figure 4](#) for $N = 7$. Even though bird and camel are facing in different directions, the interpolated shapes show the underlying transport plan essentially transports head to head, legs to legs, et cetera. As expected, the unbalanced approach yields fewer artifacts in the interpolated images.

6.3. MNIST Images. We now turn our attention to the popular MNIST dataset [\[21\]](#) which consists of handwritten digits on a 28x28 pixel grid. We simultaneously calculate multiple barycenters of four images. After selecting $\mathbb{X}_1, \mathbb{X}_2$ and $\mathbb{X}_7, \mathbb{X}_8$ from the “nine” and “six” class respectively, see the top and bottom row of [Figure 5](#), we proceed to solve a balanced UMGW problem between \mathbb{X}_i , $i = 1, \dots, 8$, where $\mathbb{X}_2, \mathbb{X}_3, \mathbb{X}_5, \mathbb{X}_6$ correspond to the barycen-

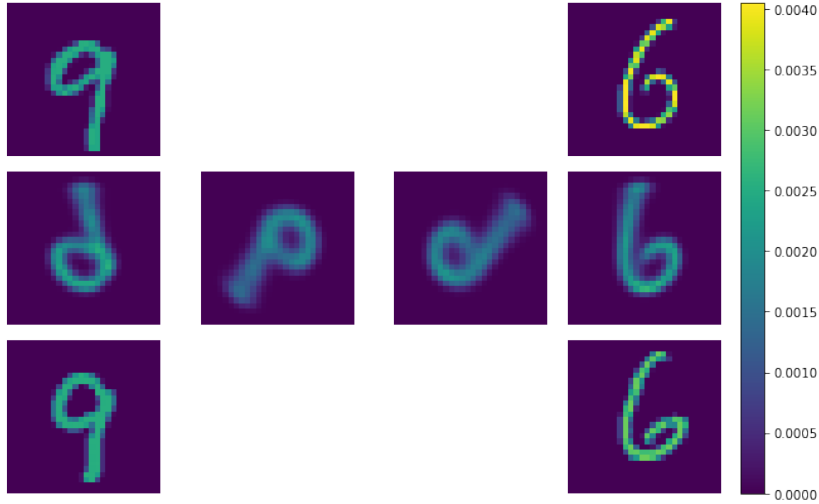


Figure 5. An interpolation (center row) between two images of the “nine” class (l.h.s. top, bottom) and two images of the “six” class (r.h.s. top, bottom).

ters for which we fix the underlying metric space to be the 28×28 pixel grid of the inputs $\mathbb{X}_1, \mathbb{X}_2, \mathbb{X}_7, \mathbb{X}_8$. More precisely, we set $\phi_1 = \phi_2 = \phi_7 = \phi_8 = \phi_{\text{bal}}$ and $\phi_3 = \dots = \phi_6 = \phi_{\text{free}}$. The cost is given by

$$c = \sum_{i=1,3} (d_i - d_2)^2 + (d_2 - d_4)^2 + (d_4 - d_5)^2 + (d_5 - d_6)^2 + \sum_{i=7,8} (d_6 - d_i)^2.$$

We apply our proposed procedure for $\varepsilon = 0.0008$. The spaces $\mathbb{X}_2, \mathbb{X}_4, \mathbb{X}_5, \mathbb{X}_6$ are shown in the center row of [Figure 5](#). Notably, $\mathbb{X}_4, \mathbb{X}_5$ progressively interpolate between \mathbb{X}_2 and \mathbb{X}_6 , which are equally close to \mathbb{X}_1 and \mathbb{X}_3 as well as to \mathbb{X}_7 and \mathbb{X}_8 respectively.

6.4. Denoising of Particle Images. In the final example, we want to remove noise from particle images. The synthetic clean images are generated by randomly choosing 40 positions in $[-1/2, 1/2]$, shifting and rotating these positions for every image, and applying a Gaussian filter. To each of the five images, we individually add noise in form of further particles to $\mathbb{X}_1, \dots, \mathbb{X}_5$. The generated images with and without noise are shown in the top and middle row of [Figure 6](#). If we would consider continuous clean images, an optimal MGW plan with respect to the cost function

$$c = \sum_{i=1}^4 |d_i - d_{i+1}|^2,$$

where d_i is again the Euclidean distance on X_i , is given by $(\text{id}, \mathcal{I}_2, \mathcal{I}_3, \mathcal{I}_4, \mathcal{I}_5)_{\#} \mu_1$, where \mathcal{I}_i describes the shifts and rotations between \mathbb{X}_1 and \mathbb{X}_i , $i = 2, \dots, 5$. Now the idea is to compute an unbalanced multi-marginal GW transport plan and consider the marginals to remove the false particles. Here we used $\phi_i = 0.0005 \phi_{\text{ent}}$, $i = 1, \dots, 5$ and $\varepsilon = 0.0002$. Considering the marginals of the computed UMGW plan shown in the bottom row of [Figure 6](#), we nearly obtain the discrete clean images back.

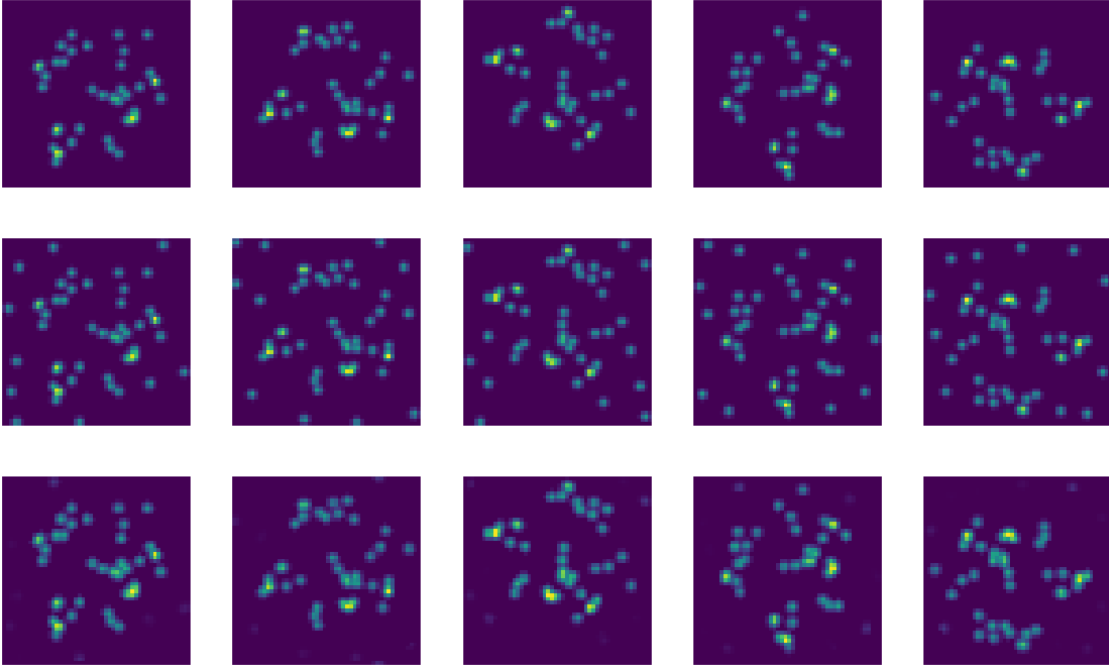


Figure 6. Top to bottom: Clean images. Noisy images $\mathbb{X}_1, \dots, \mathbb{X}_5$. Marginals of the computed UMGW plan.

Acknowledgments. The funding by the German Research Foundation (DFG) within the RTG 2433 DAEDALUS and by the BMBF project “VI-Screen” (13N15754) is gratefully acknowledged.

Appendix A. Proof of Proposition 3.1. The proof is based on properties of Csiszár divergences and the following properties of the product measure and integral operators.

Lemma A.1 (Product Measure, [8, Prop. 2.7.8]). *Let X be a Polish space. If $\pi_n \rightharpoonup \pi$ converges weakly in $\mathcal{M}^+(X)$, then $\pi_n \otimes \pi_n \rightharpoonup \pi \otimes \pi$ converges weakly in $\mathcal{M}^+(X \times X)$.*

Lemma A.2 (Lower Semi-continuity). *Let $c: X \times X \rightarrow [0, \infty]$ be lower semi-continuous. Then the mapping $\pi \mapsto \int_{X \times X} c(x, x') d\pi(x) d\pi(x')$ is weakly lower semi-continuous.*

Proof. For every lower semi-continuous c bounded from below, there exists a sequence of (Lipschitz) continuous functions $(c_k)_{k \in \mathbb{N}}$ with $c_k(x, x') \uparrow c(x, x')$ for all $x, x' \in X$, cf. [36, p. 67]. Let $\pi_n \rightharpoonup \pi$ be a weakly convergent sequence in $\mathcal{M}^+(X)$. Using Lemma A.1, we have

$$\begin{aligned} \liminf_{n \rightarrow \infty} \int_{X^2} c(x, x') d\pi_n(x) d\pi_n(x') &\geq \liminf_{n \rightarrow \infty} \int_{X^2} c_k(x, x') d\pi_n(x) d\pi_n(x') \\ &= \int_{X^2} c_k(x, x') d\pi(x) d\pi(x') \end{aligned}$$

for all $k \in \mathbb{N}$. Taking the supremum over $k \in \mathbb{N}$ and applying Lebesgue’s dominated convergence theorem establishes the weak lower semi-continuity. ■

Proof of Proposition 3.1. The objective F_ε in UMGW_ε is weakly lower semi-continuous as sum of weakly lower semi-continuous functions. More precisely, the integral is weakly lower semi-continuous by Lemma A.2. The remaining terms of the sum are compositions of weakly lower semi-continuous divergences and the weakly continuous mappings $\pi \mapsto \pi \otimes \pi$, see Lemma A.1, and $\pi \mapsto (P_{X_i})_\# \pi = \pi_i$. By Jensen's inequality, we know that for every $\mu, \nu \in \mathcal{M}^+(\mathcal{X})$ with $\|\nu\|_{\text{TV}} > 0$, it holds

$$D_\phi(\mu, \nu) \geq \|\nu\|_{\text{TV}} \phi(\|\mu\|_{\text{TV}}/\|\nu\|_{\text{TV}}),$$

see [22, (2.44)]. Therefore, we may bound the objective from below by

$$\begin{aligned} F_\varepsilon(\pi) &\geq \sum_{i=1}^N D_{\phi_i}^\otimes(\pi_i, \mu_i) + \varepsilon \text{KL}^\otimes(\pi, \nu^\otimes) \\ &\geq \sum_{i=1}^N \|\mu_i\|_{\text{TV}}^2 \phi_i\left(\frac{\|\pi_i\|_{\text{TV}}^2}{\|\mu_i\|_{\text{TV}}^2}\right) + \varepsilon \|\nu^\otimes\|_{\text{TV}}^2 \phi_{\text{KL}}\left(\frac{\|\pi\|_{\text{TV}}^2}{\|\nu^\otimes\|_{\text{TV}}^2}\right) \\ &= \|\pi\|_{\text{TV}}^2 \left[\underbrace{\sum_{i=1}^N \frac{\|\mu_i\|_{\text{TV}}^2}{\|\pi\|_{\text{TV}}^2} \phi_i\left(\frac{\|\pi_i\|_{\text{TV}}^2}{\|\mu_i\|_{\text{TV}}^2}\right)}_{\rightarrow (\phi_i)_\infty} + \varepsilon \underbrace{\frac{\|\nu^\otimes\|_{\text{TV}}^2}{\|\pi\|_{\text{TV}}^2} \phi_{\text{KL}}\left(\frac{\|\pi\|_{\text{TV}}^2}{\|\nu^\otimes\|_{\text{TV}}^2}\right)}_{\rightarrow \infty} \right]. \end{aligned}$$

For both assumptions, $F_\varepsilon(\pi)$ diverges for $\|\pi\| \rightarrow \infty$ showing coercivity. Consequently, every minimizing sequence $(\pi^{(n)})_{n \in \mathbb{N}} \in \mathcal{M}^+(X)$ with $F_\varepsilon(\pi^{(n)}) \downarrow \text{UMGW}_\varepsilon(\mathbb{X}_1, \dots, \mathbb{X}_N)$ is uniformly bounded in total variation. The theorem of Banach–Alaoglu guarantees the existence of a weakly convergent subsequence $\pi^{(k)} \rightharpoonup \tilde{\pi} \in \mathcal{M}^+(X)$. The weak lower semi-continuity of F_ε ensures that $\tilde{\pi}$ is a minimizer. ■

REFERENCES

- [1] J. M. Altschuler and E. Boix-Adsera. Polynomial-time algorithms for multimarginal optimal transport problems with decomposable structure. *arXiv:2008.03006*, 2020.
- [2] L. Ambrosio, E. Brué, and D. Semola. *Lectures on Optimal Transport*. Number 130 in Unitext. Springer, Cham, 2021.
- [3] E. Anderes, S. Borgwardt, and J. Miller. Discrete Wasserstein barycenters: optimal transport for discrete data. *Math. Methods Oper. Res.*, 84(2):389–409, 2016.
- [4] F. Beier, R. Beinert, and G. Steidl. On a linear Gromov–Wasserstein distance. *arXiv:2112.11964*, 2021.
- [5] F. Beier, J. von Lindheim, S. Neumayer, and G. Steidl. Unbalanced multi-marginal optimal transport. *arXiv:2103.10854*, 2021.
- [6] J.-D. Benamou, G. Carlier, and L. Nenna. A numerical method to solve multi-marginal optimal transport problems with Coulomb cost. In *Splitting Methods in Communication, Imaging, Science, and Engineering*, pages 577–601. Springer, Cham, 2016.
- [7] J.-D. Benamou, G. Carlier, and L. Nenna. Generalized incompressible flows, multi-marginal transport and Sinkhorn algorithm. *Numer. Math.*, 142(1):33–54, 2019.
- [8] V. I. Bogachev. *Weak convergence of measures*, volume 234 of *Mathematical Surveys and Monographs*. American Mathematical Society, Providence, RI, 2018.
- [9] E. Bogomolny, O. Bohigas, and C. Schmit. Distance matrices and isometric embedding. *J. Math. Phys. Anal. Geom.*, 4(1):7–23, 2008.
- [10] A. Carlier, K. Leonard, S. Hahmann, G. Morin, and M. Collins. The 2D shape structure dataset. <https://2dshapesstructure.github.io>.

- [11] G. Carlier and I. Ekeland. Matching for teams. *Econ. Theory*, 42(2):397–418, 2010.
- [12] Y. Chen and J. Karlsson. State tracking of linear ensembles via optimal mass transport. *IEEE Contr. Syst. Lett.*, 2(2):260–265, 2018.
- [13] M. Colombo, L. De Pascale, and S. Di Marino. Multimarginal optimal transport maps for one-dimensional repulsive costs. *Canad. J. Math.*, 67(2):350–368, 2015.
- [14] M. Cuturi and A. Doucet. Fast computation of Wasserstein barycenters. In *Proc. Mach. Learn. Res.*, volume 32, pages 685–693. PMLR, 2014.
- [15] F. Elvander, I. Haasler, A. Jakobsson, and J. Karlsson. Multi-marginal optimal transport using partial information with applications in robust localization and sensor fusion. *Signal Process.*, 171:107474, 2020.
- [16] A. Feragen, F. Lauze, and S. Hauberg. Geodesic exponential kernels: When curvature and linearity conflict. In *2015 IEEE Conference on Computer Vision and Pattern Recognition (CVPR)*, pages 3032–3042, 2015.
- [17] W. Gangbo and A. Świąch. Optimal maps for the multidimensional Monge–Kantorovich problem. *Comm. Pure Appl. Math.*, 51(1):23–45, 1998.
- [18] A. Gerolin, A. Kausamo, and T. Rajala. Multi-marginal entropy-transport with repulsive cost. *Calc. Var. Partial Differ. Equ.*, 59(3):90, 2020.
- [19] I. Haasler, A. Ringh, Y. Chen, and J. Karlsson. Multimarginal optimal transport with a tree-structured cost and the Schrödinger bridge problem. *SIAM J. Control Optim.*, 59(4):2428–2453, 2021.
- [20] K. Le, D. Le, H. Nguyen, D. Do, T. Pham, and N. Ho. Entropic Gromov-Wasserstein between Gaussian distributions. *arXiv:2108.10961*, 2021.
- [21] Y. Lecun, L. Bottou, Y. Bengio, and P. Haffner. Gradient-based learning applied to document recognition. *Proc. IEEE*, 86(11):2278–2324, 1998.
- [22] M. Liero, A. Mielke, and G. Savaré. Optimal entropy-transport problems and a new Hellinger–Kantorovich distance between positive measures. *Invent. Math.*, 211(3):969–1117, 2018.
- [23] T. Lin, N. Ho, X. Chen, M. Cuturi, and M. Jordan. Fixed-support Wasserstein barycenters: Computational hardness and fast algorithm. In H. Larochelle, M. Ranzato, R. Hadsell, M. F. Balcan, and H. Lin, editors, *Advances in Neural Information Processing Systems*, volume 33, pages 5368–5380. Curran Associates, Inc., 2020.
- [24] H. Maron and Y. Lipman. (Probably) concave graph matching. In S. Bengio, H. Wallach, H. Larochelle, K. Grauman, N. Cesa-Bianchi, and R. Garnett, editors, *Advances in Neural Information Processing Systems*, volume 31. Curran Associates, Inc., 2018.
- [25] F. Mémoli. Gromov–Wasserstein distances and the metric approach to object matching. *Found. Comput. Math.*, 11(4):417–487, 2011.
- [26] B. Pass. Multi-marginal optimal transport: Theory and applications. *ESAIM Math. Model. Numer. Anal.*, 49(6):1771–1790, 2015.
- [27] G. Peyré and M. Cuturi. Computational optimal transport: With applications to data science. *Found. Trends Mach. Learn.*, 11(5-6):355–607, 2019.
- [28] G. Peyré, M. Cuturi, and J. Solomon. Gromov-Wasserstein averaging of kernel and distance matrices. In *International Conference on Machine Learning*, pages 2664–2672, 2016.
- [29] A. Salmona, J. Delon, and A. Desolneux. Gromov-Wasserstein distances between Gaussian distributions. *arXiv:2104.07970*, 2021.
- [30] F. Santambrogio. *Optimal transport for applied mathematicians*, volume 87 of *Progress in Nonlinear Differential Equations and their Applications*. Birkhäuser/Springer, Cham, 2015. Calculus of variations, PDEs, and modeling.
- [31] I. J. Schoenberg. Metric spaces and completely monotone functions. *Ann. Math.*, 39(4):811–841, 1938.
- [32] T. Sejourne, F.-X. Vialard, and G. Peyré. The unbalanced Gromov Wasserstein distance: Conic formulation and relaxation. In *Advances in Neural Information Processing Systems*, volume 34. Curran Associates, Inc., 2021.
- [33] K.-T. Sturm. The space of spaces: curvature bounds and gradient flows on the space of metric measure spaces. *arXiv:1208.0434*, 2020.
- [34] V. Titouan, R. Flamary, N. Courty, R. Tavenard, and L. Chapel. Sliced Gromov-Wasserstein. In H. Wallach, H. Larochelle, A. Beygelzimer, F. Alché-Buc, E. Fox, and R. Garnett, editors, *Advances in Neural Information Processing Systems*, volume 32. Curran Associates, Inc., 2019.

- [35] V. Titouan, I. Redko, R. Flamary, and N. Courty. Co-optimal transport. *Advances in Neural Information Processing Systems*, 33:17559–17570, 2020.
- [36] C. Villani. *Optimal Transport: Old and New*, volume 338. Springer, 2008.
- [37] J. von Lindheim. Simple approximative algorithms for free-support barycenters. *arXiv:2203.05267*, 2022.
- [38] H. Wendland. *Scattered Data Approximation*, volume 17 of *Cambridge Monographs on Applied and Computational Mathematics*. Cambridge University Press, Cambridge, 2004.